1-1-1993

Determination of Molecular Dissociation Rates from Measurements of Scattered Solar Ultraviolet Light

K. V. Montierth

K. D. Baker
Utah State University

L. L. Jensen
Utah State University

L. R. Megill
Utah State University

JOURNAL OF GEOPHYSICAL RESEARCH, VOL. 98, NO. D5, PAGES 9011–9022, MAY 20, 1993

DETERMINATION OF MOLECULAR DISSOCIATION RATES FROM MEASUREMENTS OF SCATTERED SOLAR ULTRAVIOLET LIGHT

K. V. Montierth, Jr.

Ogden Air Logistics Center, Hill Air Force Base, Utah

K. D. Baker, L. L. Jensen, and L. R. Megill

Utah State University, Logan

Abstract. Scattered solar ultraviolet light in the spectral region from 250 to 320 nm was measured from a balloon platform at altitudes ranging from 14.5 to 38.8 km with a wavelength resolution of approximately 0.3 nm and an accuracy in determining the wavelength position of 0.5 nm. We used these scatter data to compare and validate a single scattering model developed for this purpose. Using these semi-empirical results, we constructed the single scattered component of the ultraviolet irradiance as a function of height and wavelength. From these data, it is possible to determine the percentage dissociation rate of a variety of species due to scattered ultraviolet radiation. These results are presented as a ratio of intensities $R = I_1/(I_0+I_1)$, where I_1 is the first order scattering and I_0 is the direct attenuated radiation from the sun. The attenuated direct radiation from the sun can be multiplied by the factor 1/(1-R), the Rayleigh amplification ratio used by Nicolet et al. (1982), to include the contribution to the irradiance from first order scattered light. The results are multiplied by a cross section of the species under consideration to obtain the dissociation rates. Ozone overburden and an approximate ozone particle density altitude profile are obtained when validating the single scatter model.

Introduction

In the formulation of atmospheric photochemical effects, one important parameter is the rate at which solar radiation dissociates molecules. This term, commonly called the J-value, varies widely with atmospheric conditions, latitude and time. In calculating the dissociation rates, the total radiation incident on a volume of air must be determined. The total radiation resulting from solar illumination is composed of several components: primary solar radiation, radiation scattered in the atmosphere and radiation reflected from the Earth's surface. This paper presents the analysis of scattered solar ultraviolet flux measurements over the spectral wavelength range of 250- to 320-nm from a balloon-borne spectrometer at altitudes between 14.5 and 38.8 km. From these measurements, the contribution of scattered radiation to dissociation rates in the 250 to 320-nm spectral range was determined.

We measured the intensity of the scattered or diffuse component of the solar flux in this region for many different viewing directions. This paper compares the measured scatter radiance values with predictions from a radiative transfer calculation to determine the integrated ozone column density and to validate the radiation transport model. In our observations, the spectrometer always pointed away from the Earth. As a result, the observations did not allow direct determination of the solar radiation reflected from the Earth's surface (albedo); therefore, this component is not included in the calculations. Instead, we used the works of Meier et al. [1982] and Nicolet et al. [1982] to estimate the effect of the Earth's albedo in our scattering calculation.

The increase in flux due to albedo at a solar zenith of zero degrees varies at 20 km from approximately a 7% increase at 310 nm to approximately 20% at 320 nm. At 40 km it varies from 0% at 310 nm to approximately 10% at 320 nm. The effect of albedo is negligible below 310 nm. Therefore, albedo considerations were only important to our work around 320 nm, the same wavelength region where multiple scattering becomes important. We then used the validated radiation transport model to determine the size of the first order scattering correction to the dissociation rates for minor atmospheric constituents.

Paper number 93JD00254.
0148-0227/93/93JD-00254$05.00

Experiment

An ultraviolet spectrometer onboard a balloon platform, Stratcom 7, flown from Holloman Air Force Base, New Mexico, on September 28, 1976 obtained the data base reported here. Personnel of the Atmospheric Sciences Laboratory at White Sands Missile Range, New Mexico, organized this flight. Launch occurred at 0630 MDT with the balloon reaching a float altitude of 38.8 km at about 1015. The balloon was then vented and slowly descended to 18 km by about 1600. Data were collected from launch until sunset; however, only representative data samples will be presented here. The entire data set of scattered solar flux measurements mapping the ultraviolet sky between 14.5 and 38.8 km and 250 to 320 nm are available on magnetic media from the authors.

The spectrometer consisted of two Jarrel-Ash model 82-410, 1/4-m Ebert monochrometers mounted in series to reduce the effect of light scattering in the monochrometer [Barlow and Jensen, 1976]. In this set up, the effect of scattered light was less than 1%. The monochrometers had gratings with 2360 lines/mm and a 300-nm blaze. Figure 1 shows the light path through the spectrometer and the layout of the optical components. Figure 2 shows the tandem spectrometer and the supporting electronics as a

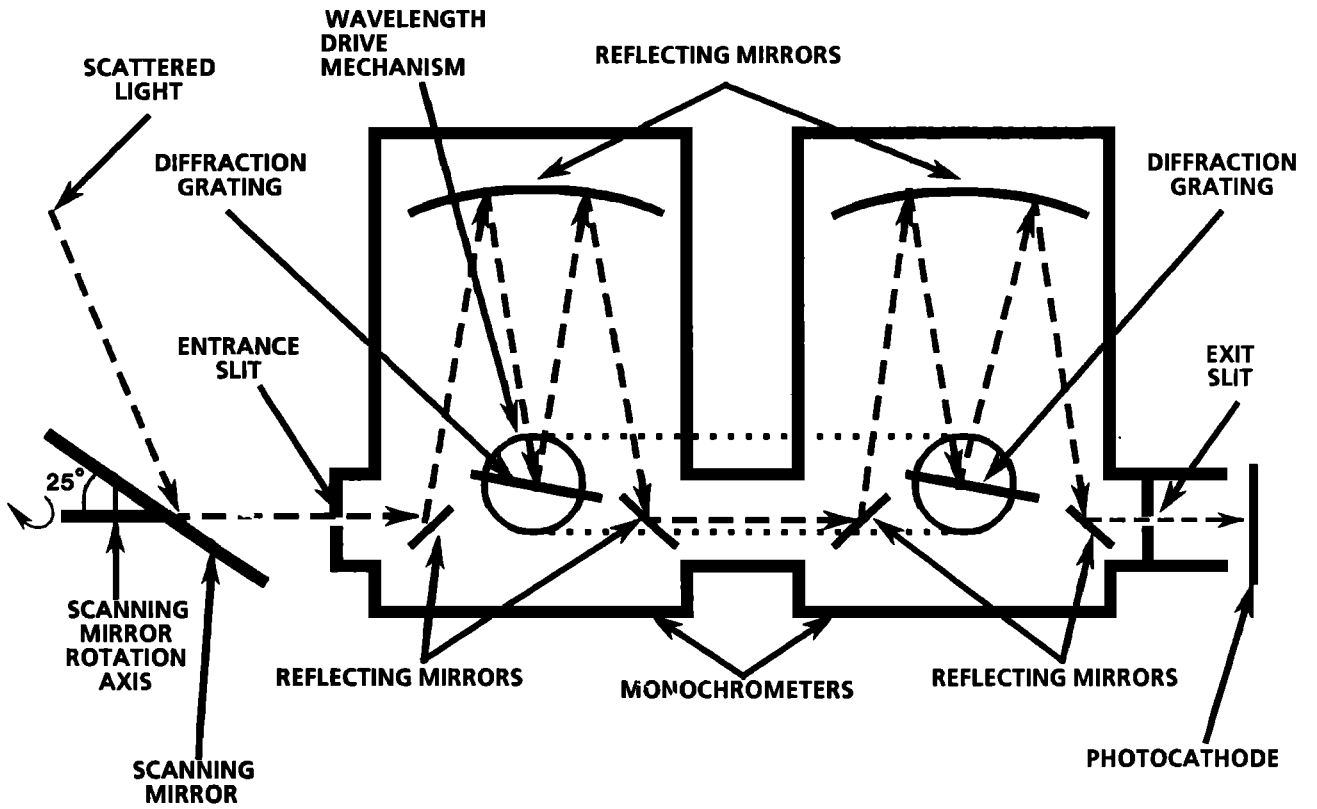

Fig. 1. Tandem spectrometer light path.

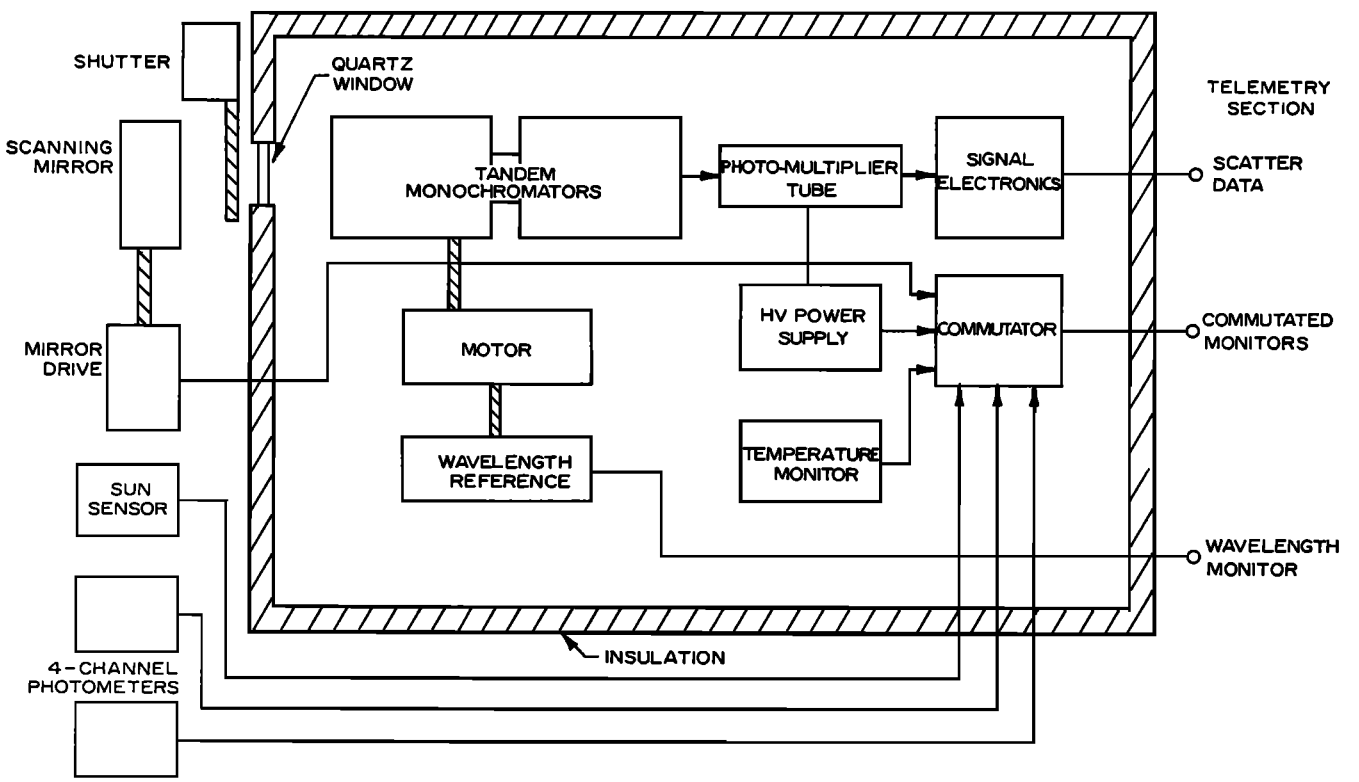

Fig. 2. Block diagram of the scanning spectrometer.

block diagram. A single stepping motor, connected to the gratings by a toothed belt, simultaneously scanned the monochrometers. The gearing determined the absolute wavelength accuracy of the passband at approximately 0.5 nm. Instrument resolution was about 0.3 nm.

A rotating mirror, placed on a platform tilted 25° with respect to the optical axis of the instrument, controlled the viewing direction of the instrument. Figures 1 and 2 show the relationship of this mirror, labelled scanning mirror, to the tandem monochrometers. Figure 3 shows how the scanning mirror controls the viewing geometry as it moves about its rotation axis. The instrument field of view was approximately circular with a half angle of about 4°. The mirror stepped through seven positions, giving the following values for the zenith angle of the center of the field of view: 40, 42, 48.5, 57.2, 67.5, 78.5, and 90°.

Payload rotation determined the azimuth direction of the instrument field of view as it ascended. A photodiode solar sensor measured the rotation to an accuracy of 1°. No attempt was made to control payload azimuth.

An ultraviolet sensitive, Hammamatsu R431 "solar-blind" photomultiplier was used in a pulse-counting mode. A shutter placed between the collecting mirror and the first monochrometer was activated between alternate spectral scans to monitor the phototube dark current levels during flight. The dark count did not change appreciably with time during the flight.

We calibrated the instrument using an Optronics Laboratory L -39 quartz halogen tungsten lamp and a deuterium lamp secondary standard, designation B7595, calibrated by the National Bureau of Standards. Uncertainties in absolute radiance values for the Optronics laboratory L-39 lamp were less than 8% [Optronics Laboratory, 1973]. The estimated uncertainty in absolute spectral irradiance for the National Bureau of Standards deuterium lamp was 6% at all wavelengths. The relative spectral irradiance of the deuterium lamp (ratio of the spectral irradiance of any two adjacent wavelengths) is 1% + .02% times the nm difference of the two wavelengths [U.S. Department of Commerce, 1976]. The deuterium lamp was used for calibration with the absolute values checked against the quartz halogen lamp at the wavelength where the two lamps had the same output based on their respective calibration reports.

For our calibration, the instrument response to the quartz halogen lamp and the deuterium lamp agreed to better than 1%. Use of both calibration lamps allowed greater relative accuracy with a higher degree of confidence in the absolute calibration. The 0.5-nm uncertainty in the location of the instrument passband produced less than a 1% error in the instrument calibration based on the reported radiance values of the calibration lamps.

Since the instrument looked at scattered or diffuse radiation from the sky rather than direct solar radiation, the light was polarized. With a reflecting mirror to change the instrument viewing direction, instrument polarization had

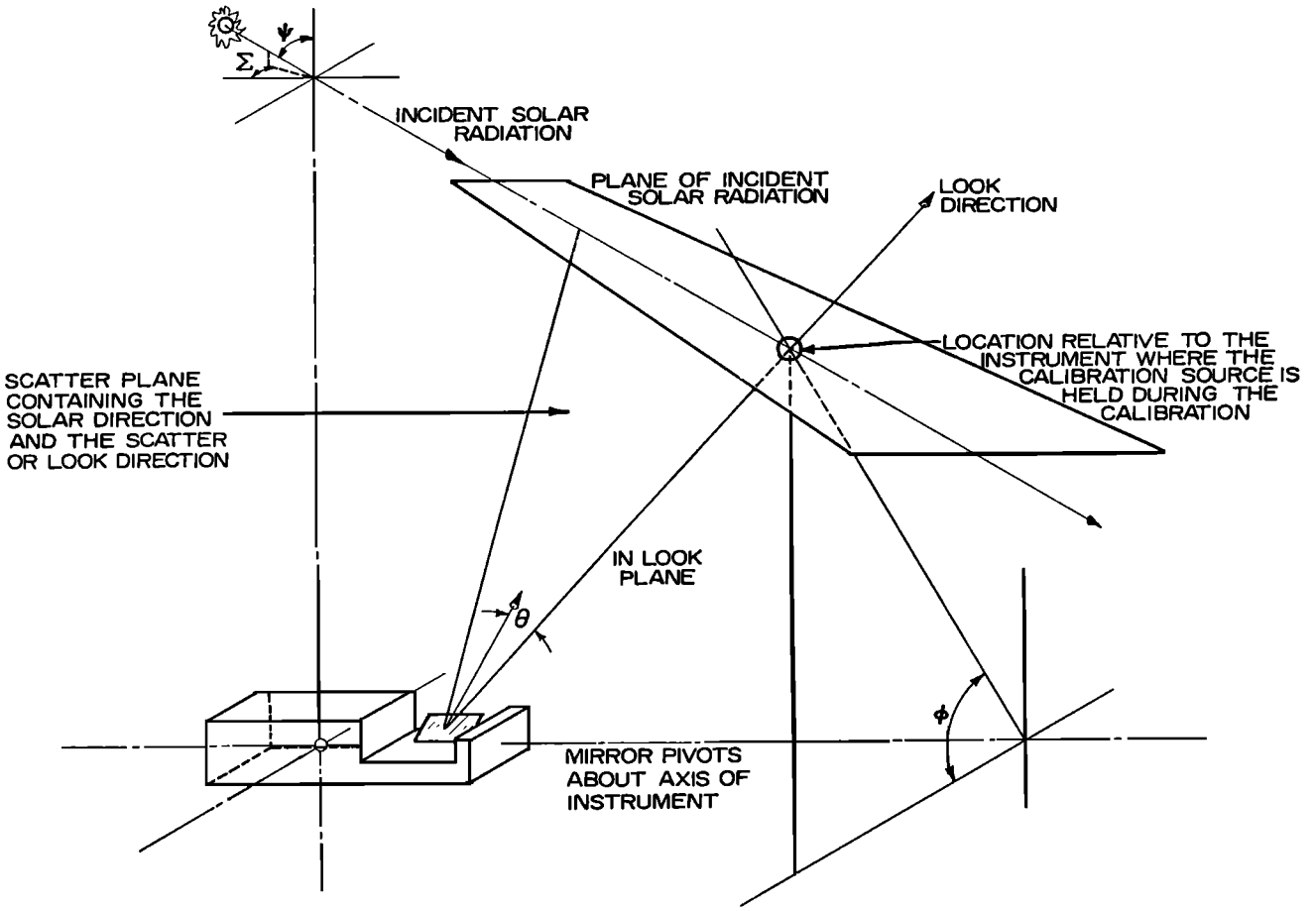

Fig. 3. Look geometry for the scanning spectrometer.

to be accounted for in the calibration process. Accordingly, we determined instrument response for two orthogonal polarization states of the calibration source and for the unpolarized calibration source for each of the seven instrument mirror positions. This calibration procedure is outlined in detail in Montierth [1982]. A comparison of instrument response to the polarized and unpolarized source determined that the measured polarizer transmission function differed by less than 1% for all calibration runs at wavelengths greater than 250 nm, where the polarizer was effective. This procedure also allowed us to apply the calibration independent of the polarizer transmission function. We did not measure light polarization for this flight but calculated it from Rayleigh scattering theory.

We used the deuterium lamp as a point source to determine the sensitivity of the spectrometer across its field of view. For the calibration, we placed the deuterium lamp in the field of view of the instrument where the maximum number of counts was observed. Placing the point source in the center of the field of view, rather than integrating across the instrument field of view between half power points, introduced an error of less than 8%. Counting statistics account for less than a 2% error.

Abnormally large signals were obtained during the flight when the collecting mirror was exposed to direct sunlight, due to scattered light from the mirror surface. These spurious signals were easily identified and the data eliminated, resulting in a loss of about 5% of the collected data. From the above discussion, we estimate the absolute error in the scatter radiance values measured by the scanning spectrometer to be less than 15%.

Theory and Analysis Procedures

To determine the first order scattering contribution to the minor constituent dissociation rate, we developed a model to calculate radiance values for the conditions measured by the scanning spectrometer. To construct this model, we solved the radiation transport equation for the appropriate parameters, allowing a direct comparison with the experimental data. This comparison provided a means of validating the theoretical model. We restricted our work to data in the 250- to 320-nm wavelength region and the 14.5- to 38.8-km altitude region when the instrument was viewing away from the Earth. The physical processes we considered were first order scattering and molecular absorption.

The only scattering process included in the model was primary Rayleigh scattering, the dominant scattering process in the altitude and wavelength region of concern. We neglected the attenuation of radiation by Mie scattering from aerosol particles out of the instrument line of sight since it would be negligible in the 14.5- to 38.8-km altitude region based on Elterman's [1968] model. We also inferred from this that Mie scattering into the instrument line of sight was negligible.

Several authors show that multiple scattering, both Rayleigh and Mie, is negligible in the wavelength and altitude region considered here, except for the radiation between 310 and 320 nm [Dave and Furukawa, 1966; Aruga and Igarashi, 1976; Luther and Gelinas, 1976; Meier et al., 1982; Nicolet et al., 1982]. For this radiation, the multiple scattering contribution varies from a few percent of the total at 310 nm to a worst case of approximately 50% at 320 nm. For wavelengths below 310 nm where multiple scattering plays a role, the absorption is so strong that these regions are not a factor in our analysis. For the region between 310 and 320 nm, the upward-streaming component of the radiation is effected more by multiple scattering than the downward-streaming component. Since the instrument in this experiment was always looking either horizontally or upward, we primarily measured downward-streaming scattered radiation.

In the 250- to 320-nm wavelength region, the primary photoabsorption is due to photolysis of ozone. To properly include this species in the radiation transport calculation, we considered the ozone cross data of Inn and Tanaka [1959], Molina and Molina [1986], and the World Meteorological Organization (WMO) [1986]. The WMO recommendation, based on the results of Paur and Bass [1985], agrees with both the Molina and Molina [1986] and the Inn and Tanaka [1959] measurements in our wavelength region of interest to within 3%, with the Molina and Molina [1986] cross sections being slightly larger. As a result, we used Inn and Tanaka's [1959] cross sectional data since these values are representative over the wavelength region considered and have been used in a previous work we used for comparison.

For the solar radiance values at the top of the atmosphere, we considered the data of Arveson et al. [1969], Broadfoot [1972], Donnelly and Pope [1973], Brasseur and Simon [1981], Hall [1981], Mentall et al. [1981], Mount and Rottman [1983], Mount and Rottman [1985], Mentall and Williams [1988], and Anderson and Hall [1989]. Nicolet [1989] shows a comparison of the principal observational results over 1-nm intervals for the 10 years prior to his paper. He indicates that the general accuracy of the solar spectral irradiances cannot be better than plus or minus 10 to 15%.

We used Mentall and Williams's [1988] solar flux data (December 10, 1984 rocket flight). Mentall and Williams [1988] cover the solar irradiance values for our entire wavelength region with a single source measurement. Mentall is also the experimenter we compared our measurements with later in this paper.

We assumed that the total particle density had an exponential distribution:

$$N(y) = n_0 e^{-y/h} \tag{1}$$

where n_o is number density at y = 0 (2.906×10^{19} cm^{-3}), y is distance above the earth (mean sea level) (km), and h is scale height (7.08 km).

We used the Fermi-Dirac distribution function in conjunction with the exponential distribution taken from Shettle and Green [1974] to determine the ozone distribution. In our model, we used Shettle and Green's distribution primarily to define the shape of the ozone profile. We determined the magnitude of the total ozone column content as part of the analysis procedures.

$$N(y) = n_1(y) + n_2(y) \tag{2}$$

$$n_1(y) = (\omega_0'/h')e^{-y/h'}$$

$$n_2(y) = (\omega_0/h)\left(\frac{e^{(y-y_p)/h}}{[1+e^{(y-y_p)/h}]^2}\right)$$

where ω_0 is 0.218 cm, h is 4.63 km, ω'_0 is 0.0127 cm, h' is 5.78 km, y_p is 23.25 km, and y is vertical altitude, km.

To solve the radiation transport equation with the above physical processes applied, we determined the radiation reaching the instrument which is scattered from the volume ΔV and then obtained the total scattered radiation by summing along the look direction of the instrument (see Figure 4). Variations across the volume ΔV were ignored since they can be shown to be negligible [Montierth, 1982]. We followed Chandrasekhar's [1960] development for Rayleigh scattering assuming incident unpolarized radiation on the volume ΔV and including the molecular anistropy, which results in equation (3). We determined the molecular polarizability, α, of the air molecules from the Clausius-Mossotti equation for dilute substances. Again, this is consistent with Chandrasekhar [1960].

$$I_{ins} = A_{slit}\Delta\omega'''\Delta\omega''\int_S^{\infty} N(S')\sigma_{R\omega}I_{\infty}(\lambda)e^{-t_1(S',\infty)}e^{-t_2(S,S')}dS_2$$

$$\sigma_{R\omega} = \left(\frac{32\pi^4}{3\lambda^4}\right)\alpha^2 1.06[0.7629(1+0.9324\cos^2\omega)]cm^2 \quad (3)$$

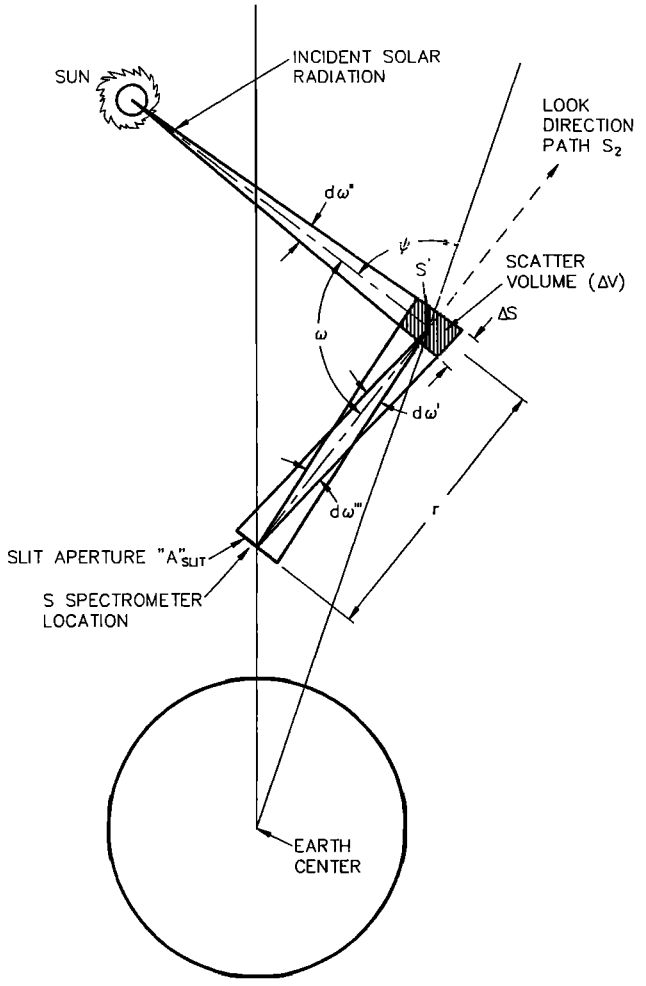

Fig. 4. Instrument look geometry showing the relationship of the instrument field of view to the scatter volume and the solid angle of incident solar radiation. Integration geometry for the radiation transport equation.

where A_{slit} is slit aperature, S_2 is look path, ds_2 is integration along the look path, S is spectrometer location, S'is an arbitrary point on the look path, t_1 is the optical depth between the sun and the point S' on the look path along the path from the sun to the look path, t_2 is the optical depth between S and S' along the look path, $\Delta\omega'''$is the solid acceptance angle of the instrument $\Delta\omega''$ is the solid angle of incident pencil of radiation, N(S') is total number density at the point (S'), and ω scatter angle.

The solar zenith angle at each point on the integration path is represented by ψ, while ω represents the scattering angle. For this integration, we considered an earth-centered spherical geometry. Figure 4 shows the relationship between the solid angle subtended by the instrument, the instrument look angle, the solid angle of the incident solar radiation, and the elemental scattering volume. A detailed description of the development of equation (3), including an evaluation of the optical depth terms for the assumed spherical geometry and the integration of equation (3), can be found in Montierth [1982]. This expression can be integrated numerically using standard techniques, providing a theoretical calculation of the expected radiation levels. These results are then expressed in kR/nm for comparison with the measured data.

Analysis And Results

We first reduced the raw flight data to radiance values as a function of wavelength, instrument look direction and altitude. We then used these data to determine the vertical ozone column density, overburden, above the observation point by comparing the shape of the measured spectra with the shape of the theoretical spectra. We made this comparison by assuming a value for the ozone overburden in the model, calculating theoretical spectra for the same circumstances as the measured spectra, then normalizing the theoretical spectra to those measured. The uncertainty in wavelength position was removed where possible by lining up solar lines in the measured and model-generated data. We allowed the ozone overburden to vary in the theoretical model, producing a family of spectral curves normalized to the measured spectra at the same wavelength value. We then used a sequential search optimization algorithm to search for the theoretical spectra that gave the best fit to the measurements over the 270 to 305-nm wavelength region. This gave the ozone column density which produced the best fit to the measured spectra. The optimization algorithm sought the theoretical curve which had the smallest value for the following:

$$A = \sum^{\infty} ((R_i^{measured} - R_i^{theoretical})/R_i^{measured})^2 \quad (4)$$

where Σ is summation across a spectral scan, $R_i^{measured}$ is measured radiation at wavelength i, and $R_i^{theoretical}$ is model-produced radiation at wavelength i where the sum is performed over a spectral scan.

The convergence criteria for the optimization algorithm was approximately 1.5% of the integrated ozone column density. We performed this comparison on data in the 270- to 300-nm wavelength region at float altitude, avoiding

wavelengths greater than 305 nm, where the measured scatter radiance values are relatively insensitive to changes in the ozone column content. We also wanted to avoid the region between 250 and 270 nm, which is extremely sensitive to changes in ozone column content above the measurement point. As the altitude decreased, we increased the lower limit on the wavelength interval in order to avoid regions extremely sensitive to changes in ozone column content. This avoided regions where the signal was small. We also increased the upper limit on the wavelength interval used to 305 nm at lower altitudes; the wavelength interval we used for ozone determination at 20 km was 295 to 305 nm. These choices provided a reasonable data set at each altitude.

We found that the optimization algorithm determined the same ozone overburden to within 5%, regardless of the wavelength value chosen for the normalization process, giving confidence to the measurement. This optimization algorithm also converged to the same ozone value within 7% (one standard deviation) for the data scans at float altitude, where many spectral scans exist. We varied the scale height for the ozone distribution used in the calculation to determine the effect of the shape of the ozone profile on the calculation. We found that the shape of the assumed ozone profile in the model had no significant effect in determining the theoretical scattering values or the ozone overburden for the data presented here. However, the shape of the assumed ozone profile will effect the results near sunset or sunrise. If the 15% worst case error estimate in the measured flux values were totally a relative error over the range of wavelengths used in ozone estimation, the error produced in ozone determination would be less than 6%. From the above discussion, we estimate the uncertaintity in the integrated column density to be in the range of 6 to 7%.

The model was validated in an absolute sense by determining the factor required to scale the model-generated data to the measured data. This was determined by using the vertical ozone column densities derived here and comparing the model-produced radiance values to the measured radiance values for each data scan at the wavelength point in each scan previously used for normalization in the vertical column density determination. Table 1 shows these scaling terms. The average of the scaling values from Table 1 is 1.000 with a standard deviation of 0.170. This table shows the uncertaintity in absolute value between our model-calculated values and the measured data. The standard deviation of 0.170 presented in Table 1 is a cumulative uncertainty in the experiment. This includes calibration errors, instrument errors and model uncertainties, such as the solar flux and ozone cross sections used in the model calculations for all of the instrument look directions in the 14.5- to 38.8-km altitude region. The 17% for one standard deviation unit uncertaintity is within the cumulative error of this experiment. It is also consistent with a 6 to 7% uncertaintity in the integrated ozone column density.

Figure 5 shows the relative comparison between the measured and model-produced data with the model-produced data scaled with the values presented in Table 1 for eight cases of solar zenith angle, altitude, and instrument look zenith angle. The solar azimuth angles indicated on Figure 5 are referenced to the optical axis of

TABLE 1. Final Normalization Scale Factors as a Function of Altitude and Look Angle

Look Angle, deg		Altitude, km		Scale Factor	
78.5	48.5	19.8	21.5	1.188	1.308
		38.7	32.8	1.066	1.026
				(Fig. 5e)	(Fig. 5d)
			30.6		1.210
			24.5		1.044
67.5	42.0	26.0	17.3	1.082	0.998
		29.7	21.5	0.981	0.998
				(Fig. 5c)	(Fig. 5b)
		35.0	22.3	1.034	0.818
		36.4	38.7	1.094	1.052
		31.6	38.4	1.158	0.954
		24.8		1.248	(Fig. 5f)
			36.0		0.784
					(Fig. 5g)
			32.2		0.756
			26.0		1.062
			19.8		1.028
					(Fig. 5h)
57.2	40.0	15.5	17.3	1.332	1.166
		23.2		0.892	(Fig. 5a)
		36.4	28.0	1.056	0.642
		37.9	38.7	0.984	0.892
		36.2	32.2	1.070	0.758
		32.1	28.9	1.034	0.572
		27.0	28.9	0.822	0.986
			22.4		0.987

Mean = 1.000 and standard deviation = 0.170.

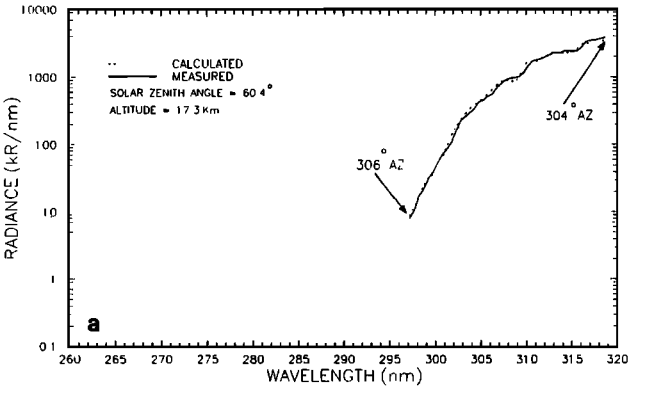

Fig. 5. Comparison of model-produced radiances and measured radiances with the model-produced radiances scaled to the measured radiances (see Table 1 for scaling factors) for (a) 40° look zenith angle, 17.3 km altitude; (b) 42° look zenith angle, 21.5 km altitude; (c) 67.5° look zenith angle, 29.7 km altitude; (d) 48.5° look zenith angle, 32.8 km altitude; (e) 78.5° look zenith angle, 38.7 km altitude; (f) 42° look zenith angle, 38.4 km altitude; (g) 42° look zenith angle, 36.0 km altitude; and (h) 42° look zenith angle, 19.8 km altitude. The solar zenith angles, solar azimuth angle and altitude are indicated on each figure.

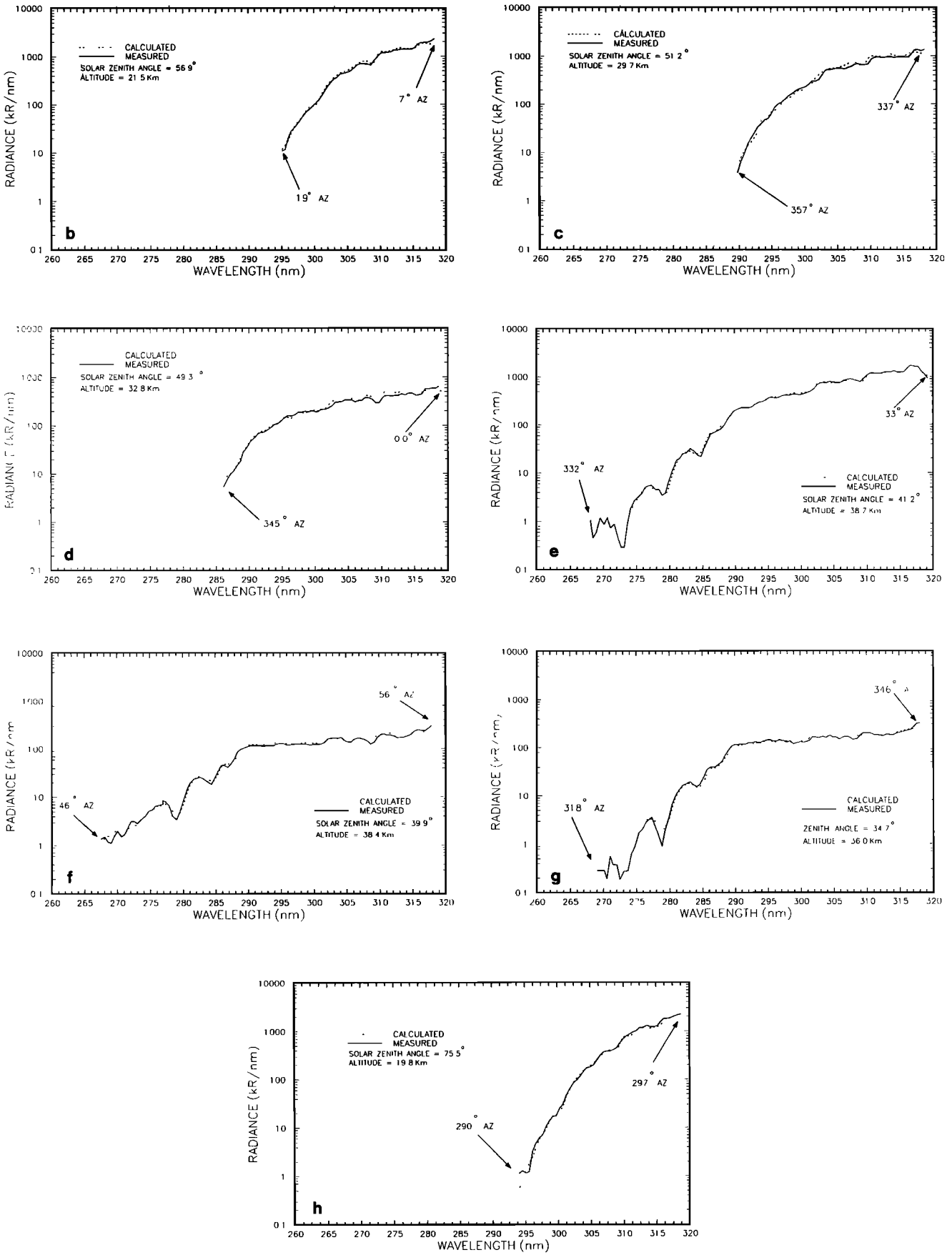

Fig. 5. (continued)

the spectrometer. Zero degrees is with the sun behind the instrument (relative to the scanning mirror); the angles increase clockwise from this reference, looking down on the instrument. The scale terms used for the model data given in Figure 5 are indicated in Table 1. As shown in Figure 5, the relative agreement between the measured and model-produced data is good. This comparison, both absolute and relative, is taken as a validation of the single scatter model used in this work. The results shown here are representative of a larger data set; other cases, as well as the radiative transport model, written in Fortran, are available from the authors.

We compared the ultraviolet spectra measured in this experiment and the theoretical spectral values produced by the model with the results of other experimenters to provide additional validation [Dave and Furukawa, 1966, Meier et al., 1982, Nicolet et al., 1982; Herman and Mentall, 1982]. The works of Meier et al. [1982] and Nicolet et al. [1982] present limited data with no albedo, the conditions of this experiment. Comparison of our results with Nicolet et al. [1982] are detailed later in the paper.

Comparisons of our results with data presented by Herman and Mentall [1982] are presented in Figure 6. Figure 6a shows the similarity between Herman and Mentall's data collected at 40 km at a horizontal look direction with the data our instrument collected at 38.7 km at a 78.5° look zenith angle. Given the difference in viewing geometry and the approximately 1.3-km difference in altitude where the data were collected, and, therefore, a difference in the ozone column density for the two data sets, our data is consistent with that of the Herman and Mentall [1982].

Figure 6b compares the upward- and downward-streaming radiation components Herman and Mentall [1982] collected at 40 km with results from our instrument with a 42° look zenith angle at 38.4 km. For this viewing geometry, the data collected by our instrument, which was predominately downward-streaming radiation, is similar to Herman and Mentall's [1982] downward-streaming radiation. Given the difference in look geometry and the approximately 1.5-km difference in altitude where the data were collected, the comparison of our data with that of Herman and Mentall [1982] is good and the best comparison we can make.

Figure 7 shows the results of the ozone overburden determination. If we extrapolate our ozone overburden values to 40 km, we obtain approximately the same overburden that Herman and Mentall [1982] obtained at 40 km, 2.69 x 10^{17} particles/cm^2. At 38.7 km the value we determined was 3.5 x 10^{17} particles/cm^2. The difference in altitude can explain the deviation in both shape and absolute value between the two data sets as illustrated in Figure 6. There are also differences caused by the different geometry of the two measurements.

We obtained a rough ozone particle density as a function of altitude by fitting a function to the ozone overburden values and then spatially differentiating this function, giving the results shown in Figure 8. The data presented in Figure 8 are only given as a relative comparison of the ozone values obtained here with those of the other instruments carried onboard the same balloon

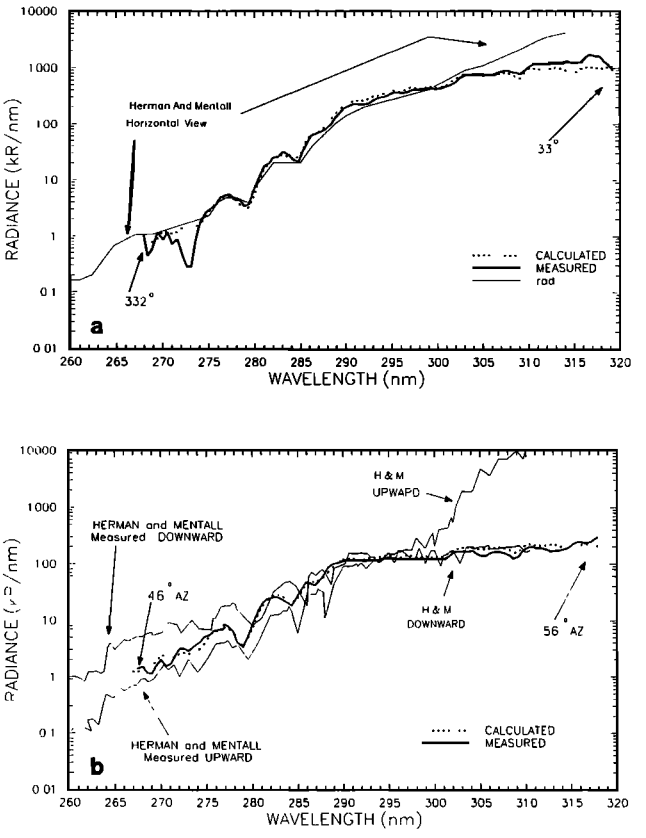

Fig. 6. Comparison of our measured and model-produced data with the measured data of Herman and Mentall [1982]. (a) Data from Figure 5e, 78.5° look zenith angle and 38.7 km, compared with Herman and Mentall's horizontal look case at 40 km. (b) Data from Figure 5f, 40° look zenith angle and 38.4 km, compared with Herman and Mentall's upward- and downward-streaming radiation at 40 km.

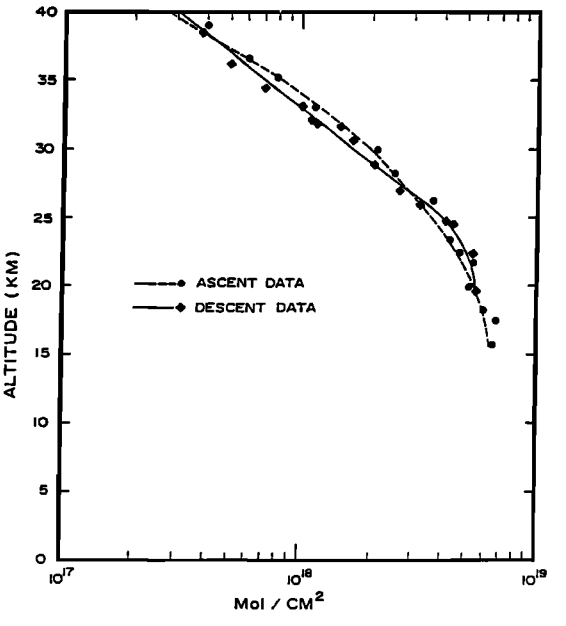

Fig. 7. Measured integrated ozone column density as a function of altitude.

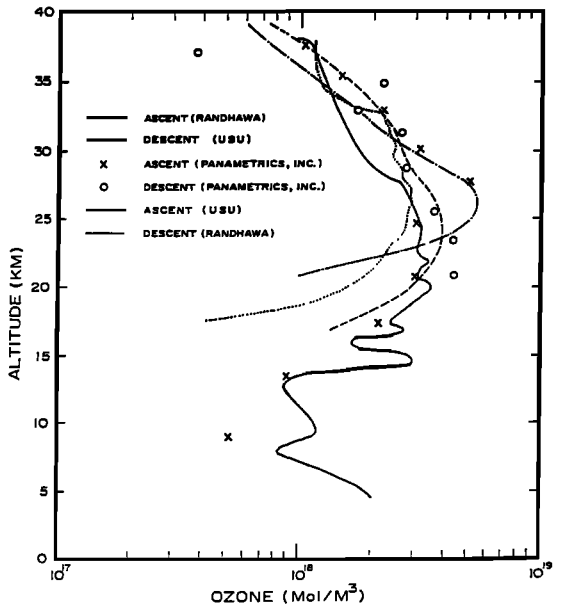

Fig. 8. Ozone number densities as a function of altitude.

flight. The process of differentiation to obtain the number densities from the integrated number densities makes it difficult to place an error estimate on these values.

As Figure 8 illustrates, there is considerable difference between the peak of the ozone profiles measured on the ascent and descent legs of the flight. The ozone profiles obtained using the above technique show general agreement with those of the other two experimenters on this flight in the locations of the upleg and downleg ozone peaks and the magnitudes of the upleg and downleg particle densities. The Panametrics instrument was a filter photometer [Sellers et al., 1977]. The other results [Randhawa et al., 1977] are from a chemiluminescent detector. As might be expected, the chemiluminescent detector yields the best spatial resolution.

Since our theoretical model was validated against the entire measured data set which covers solar zenith angles ranging from 38 to 76°, look zenith angles ranging from 40 to 90° and altitudes between 14.5 and 38.8 km for all azimuth directions of the instrument, we used the theoretical model data in place of the measured data to determine the size of the single scattered radiation through a volume of air. Use of the model-produced data was necessary because the instrument collected data for too few look directions at each altitude to perform the integration outlined and determine the total scatter radiation passing through a volume of air with measured data. The attenuated direct solar radiation was not available for this flight; the attenuated direct solar radiation as a function of altitude and solar zenith angle was determined from the validated model. We determined the total radiance passing through a scatter volume in two segments, upward- and downward-streaming radiation. The effects of multiple scattering are more significant for the upward-streaming radiation. We performed an integration of the scatter radiance values passing through the upper and lower hemispheres of a volume of air numerically, using the theoretical model for the radiance values. This integration was performed for three solar zenith angles and five altitudes. Details of this integration are contained in Montierth [1982]. The results of this integration are the total single scatter radiance passing through a volume of air as a function of altitude, wavelength, and solar zenith angle. These radiances were then used to determine the ratio of first scattered radiation to total radiation passing through a volume of air. Rayleigh amplification ratios were determined from these ratios.

Data presented in this paper may be used to compute the ratio of the dissociation radiance to the attenuated solar radiance at a given altitude, the Rayleigh amplification ratio. Equation (5) represents the ratio of first scatter radiation to total radiation, direct radiation plus single scatter radiation:

$$R_u = I_{1u}/(I_0+I_1) \quad (5)$$

$$R_d = I_{1d}/(I_0+I_1)$$

$$I_1 = I_{1U} + I_{1d}$$

where I_{1U} is upward-streaming, first scatter radiation; I_{1D} is downward-streaming, first scatter radiation; I_0 direct attenuated solar radiation; R_u is upward-streaming ratio; R_d is downward streaming ratio, and R is $R_u + R_d$. These ratios, shown in Figure 9, are broken into upward- and downward-streaming scatter radiation because our model was validated primarily for downward-streaming radiation. These ratios are independent of the solar radiance at the top of the atmosphere chosen for the model. The Rayleigh amplification ratio is constructed from these ratios by taking 1/(1-R) where R is the ratio represented in equation (5) and Figure 9. These agree with the Rayleigh amplification ratios presented in Table 5 of Nicolet et al. [1982] within a few percent for regions where multiple scattering is unimportant. Multiple scattering is important both beyond 310 nm and deep in the atmosphere where scattering becomes more important than direct radiation. Multiple scattering was not considered in our model so deviations could be larger in the region between 310 and 320 nm. The agreement between our theoretical calculations and those of Nicolet et al. [1982], based on a comparison of the Rayleigh amplification ratios, is good.

In the course of this work, we have produced a set of numbers which yields a fraction by which the attenuated solar flux can be multiplied to determine the total irradiance which, in turn, can be used to calculate the dissociation rate of a variety of molecules. To calculate the dissociation rate of any molecule when the cross section is known, the attenuated direct solar radiance may be calculated, given the ozone profile at the time, and multiplied by the quantity 1/(1-R) (the Rayleigh amplification ratio) to include the contribution to the irradiance from scattered light. Any term due to additional albedo effects may be added and the result multiplied by the cross section. This provides the dissociation rate at the wavelength where the cross section is taken. The result is the dissociation rate per molecule due to solar radiance at that wavelength.

We have also demonstrated that it is possible to determine the ozone overburden with this technique and that the apparent error (the amount by which the ozone

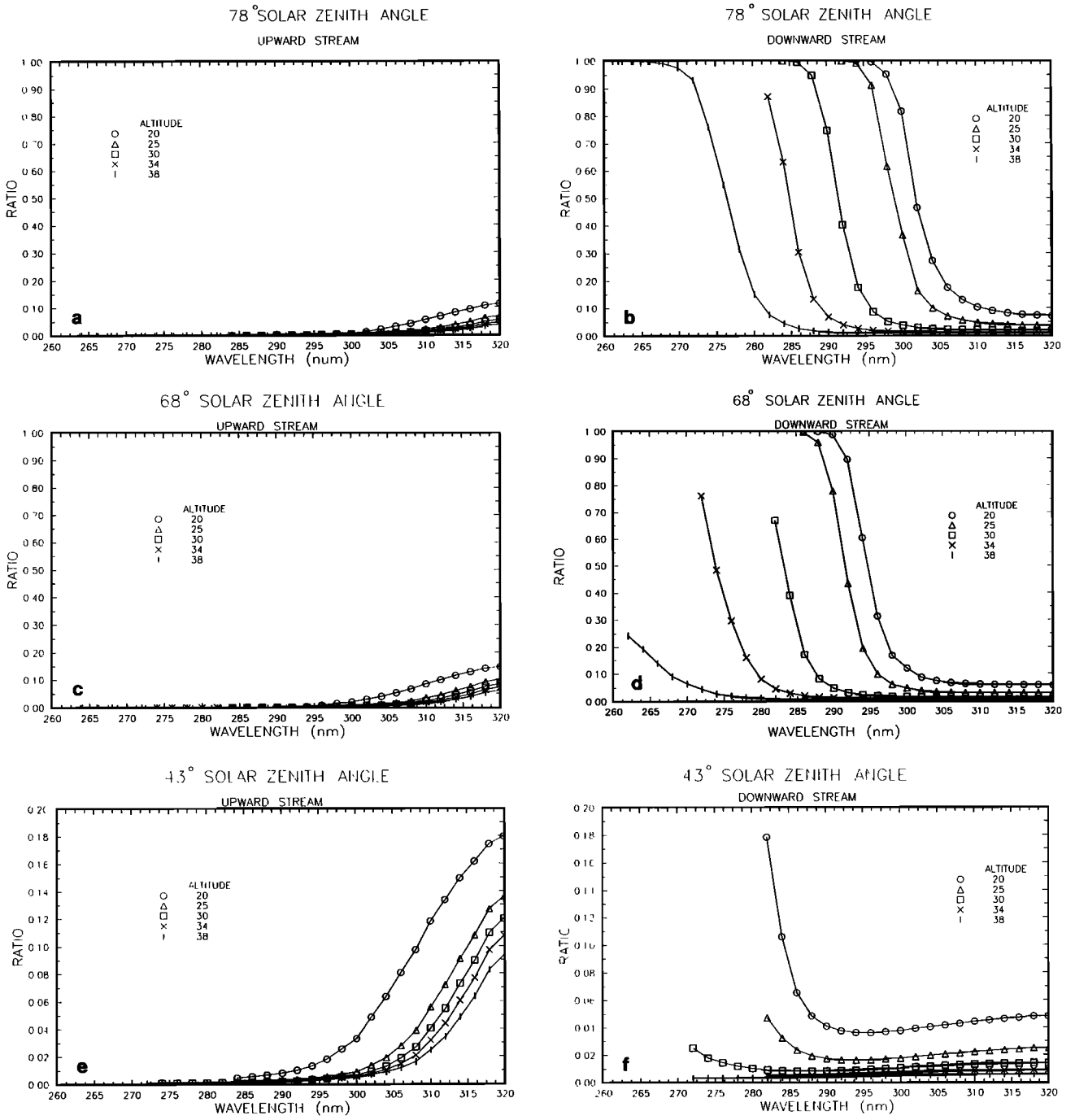

Fig. 9. Ratio of first scattering to total radiance broken into upward- and downward-streaming components for three solar zenith angles: (a) 78° upward-streaming, (b) 78° downward-streaming, (c) 68° upward-streaming, (d) 68° downward-streaming, (e) 43 ° upward streaming, and (f) 43° downward streaming. Each figure contains data for 20, 25, 30, 34, 38 km altitudes.

can be changed without significant deviation in the fit to the data) is only a few percent when many wavelengths are used for such a fit. The absolute accuracy of such a result is always limited by knowledge of the appropriate cross sections and primary solar flux.

Conclusion

This work has demonstrated that for the 250 to 320-nm wavelength range and the 14.5 to 38.8-km altitude region, a single scatter model developed here is adequate to determine the scatter corrections to minor constituent dissociation rates up to 310 nm. A simple multiplicative factor, the Rayleigh amplification ratio, can be used to include scattering in dissociation rate calculations. Reasonably accurate ozone overburden profiles can be extracted from the measured scatter radiance data using the procedure outlined in this paper.

Acknowledgements. This study was supported by the United States Army, Atmospheric Sciences Laboratory, White Sands Missile Range, New Mexico. under contract

DAEA 18-76-C-0400. Analysis support was also provided by the National Science Foundation under several grants. The solar ultraviolet spectrometer was developed with support from the Atmospheric Sciences Laboratory as a research project as part of Allen Barlow's Master of Engineering (Barlow and Jensen, 1976) program at Utah State University.

References

Anderson, G.P., and L.A. Hall, Solar irradiance between 2000 and 3100 angstroms with spectral band pass of 1.0 angstroms, J. Geophys. Res., 94, 6435-6441, 1989.

Aruga, T., and T. Igarashi, Vertical distribution of ozone: A new method of determination using satellite measurements, Appl. Opt., 15, 261-272, 1976.

Arvesen, J.C., R.N. Griffin, Jr., and B.D. Pearson, Jr., Determination of an extraterrestrial solar spectral irradiance from a research aircraft, Appl. Opt. B., 8, 2215-2232, 1969.

Barlow, A.R., and L.L. Jensen, Solar ultraviolet spectrometer final report, submitted to White Sands Missile Range, contract number DAAD07-75-C-0107, Space Sci. Lab., Utah State Univ., Logan, 1976.

Brasseur, G., and P.C. Simon, Stratospheric chemical and thermal response to long-term variability in solar uv irradiance, J. Geophys. Res., 86, 7343-7362, 1981.

Broadfoot, A. L., The solar spectrum 2100 - 3200 Å, Astrophys. J., 173, 681-689, 1972.

Chandrasekhar, S., Radiative Transfer, pp. 45-50, Dover Publications, Mineloa, N. Y., 1960.

Dave, J.V., and P.M. Furukawa, Scattered radiation in the ozone absorption bands at selected levels of a terrestrial rayleigh atmosphere, Am. Meteorol. Soc. Monograph, 7, 1966.

Donnelly, F.R., and J.H. Pope, The 1-3000A solar flux for a moderate level of solar activity for use in modeling the ionosphere and upper atmosphere, NOAA Tech. Rep. ERL 276-sel-925, 40 pp., 1973.

Elterman, L., UV, Visible and IR attenuation for altitudes to 50 km, Rep. AFCRL-68-0153, 47 pp, Air Force Cambridge Res. Lab., Bedford, Mass., 1968.

Hall, L.A., Solar ultraviolet irradiance at 40 kilometers in the stratosphere, J. Geophys. Res., 86, 555-560, 1981.

Herman, J. R., and J.E. Mentall, The direct and scattered solar flux within the stratosphere., J. Geophys. Res., 87, 1319-1330, 1982.

Inn, E.C.Y., and Y. Tanaka, Ozone absorption coefficients in the visible and ultraviolet regions, in Ozone Chemistry and Technology, pp. 263-268, American Chemical Society, Washington, D.C., 1959.

Luther, F.M., and R.S. Gelinas, Effect of molecular multiple scattering and surface albedo on atmospheric photodissociation rates, J. Geophys. Res., 81, 1125-1132, 1976.

Meier, R.R., M. Nicolet, and D.E. Anderson Jr., Radiation field in the troposphere and stratosphere, from 240-1000 nm I. General Anal. Space Sci., 30, 923-933, 1982.

Mentall, J.E., and D.E. Williams, Solar ultraviolet irradiances on December 7, 1983 and December 10, 1984, J. Geophys. Res., 93, 735-746, 1988.

Mentall, J.E., J.E. Frederick, and J.R. Herman, The solar irradiance from 200 to 330 nm, J. Geophys. Res., 86, 9881-9884, 1981.

Molina, L.T., and M.J. Molina, Absolute absorption cross sections of ozone in the 185-to-350 nm wavelength range, J. Geophys. Res., 91, 14501-14508, 1986.

Montierth, K.V. Jr., A determination of corrections required to include scattering in the evaluation of J-values, Ph.D. dissertation, Utah State Univ., Logan, 1982.

Mount, G. H. and G. J. Rottman, The solar absolute spectral irradiance at 1216 Å and 1800 - 3173 Å, J. Geophys. Res., 88, 6807-6811, 1983.

Mount, G. H. and G. J. Rottman, Solar absolute spectral irradiance 118 - 300nm, J. Geophys. Res., 90, 13,031-13,036, 1985.

Nicolet, M., Solar spectral irradiancies with their diversity between 120 and 900 nm, Planet. Space Sci., 37, 1249-1289, 1989.

Nicolet, M., R.R. Meier, and D.E. Anderson Jr., Radiation field in the troposphere and stratosphere, II, Numerical analysis, Space Sci., 30, 935-983, 1982.

Optronics Laboratories, Inc., Instructions for using the Optronic Laboratories 45-watt tungsten-halogen lamp: Standards of total and spectral irradiance, Silver Spring, Md., 1973.

Paur, R.J., and A.M. Bass, The ultraviolet cross sections of ozone II, Results and temperature dependence in atmospheric ozone, in Proceedings of the Quadrenial Ozone Symposium, Halkidiki, Greece, edited by C. Zefevoc and A. Ghazi, pp. 611-616, D. Reidel, Hingham, Mass., 1985.

Sellers, B., F. Hansen, and J. Hunervadel, Solar uv flux and total ozone measurements from Stratcom VII-A, (abstract) EOS Trans. AGU, 58, 452, 1977.

Shettle, E.P., and A.E.S. Green, Multiple scattering calculation of the middle ultraviolet reaching the ground, Appl. Opt., 13, 1567-1581, 1974.

Randhawa, J., M. Isquierdo, Z. Salpeter, and C. McDonald, Stratospheric ozone density as measured by chemiluminescent sensors during the Stratcom VII-A flight, (abstract) , *Eos. Trans. AGU, 58*, 452, 1977.

U.S. Department of Commerce, Deuterium Lamp Standard of spectral irradiance, National Bureau of Standards, Washington, D. C., Oct. 22, 1976.

World Meteorological Organization, Atmospheric Ozone 1985, Assessment of our understanding of the processes controlling its present distribution and changes, Rep., 16, Global Ozone Res. and Monitoring Project, Geneva, Switzerland, 1986.

K. D. Baker, L. L. Jensen, and L. R. Megill, Utah State University, Logan UT 84322-4437.

K. V. Montierth, Jr., Department of the Air Force, Ogden Air Logistics Center (AFMC), Hill Air Force Base, UT 84056.

(Received January 24, 1992;
revised December 30, 1992;
accepted January 24, 1993.)